

# A GOOD MASS PROXY FOR GALAXY CLUSTERS WITH XMM-Newton

Hai-Hui Zhao, Shu-Mei Jia, Yong Chen, Cheng-Kui Li, Li-Ming Song, Fei Xie

## ABSTRACT

We use a sample of 39 galaxy clusters at redshift  $z < 0.1$  observed by *XMM-Newton* to investigate the relations between X-ray observables and total mass. Based on central cooling time and central temperature drop, the clusters in this sample are divided into two groups: 25 cool core clusters and 14 non-cool core clusters, respectively. We study the scaling relations of  $L_{\text{bol}}-M_{500}$ ,  $M_{500}-T$ ,  $M_{500}-M_{\text{g}}$  and  $M_{500}-Y_{\text{X}}$ , and also the influences of cool core on these relations. The results show that the  $M_{500}-Y_{\text{X}}$  relation has a slope close to the standard self-similar value, has the smallest scatter and does not vary with the cluster sample. Moreover, the  $M_{500}-Y_{\text{X}}$  relation is not affected by the cool core. Thus, the parameter of  $Y_{\text{X}}$  may be the best mass indicator.

*Subject headings:* galaxies: clusters: general — X-rays: galaxies: clusters — intergalactic medium

## 1. Introduction

Cluster mass is a key parameter for us to explore the evolution of large-scale structure of the Universe and to test the cosmological models (Voit & Donhue 2005; Vikhlinin et al. 2009; Mantz et al. 2010; Reichert et al. 2011). The commonly-used method of X-ray mass estimate is assuming that the clusters are spherically symmetric and the intracluster medium (ICM) is in hydrostatic equilibrium within the cluster gravitational well (Sarazin 1988). But for some cases, like high-redshift, dynamically unrelaxed or X-ray faint clusters, the common X-ray mass estimate is not suitable. In these cases, the cluster mass can be inferred from the relations between the total mass and observables, such as luminosity ( $L_{\text{X}}$ ), X ray temperature ( $T$ ), gas mass ( $M_{\text{g}}$ ), and total thermal energy of the ICM ( $Y_{\text{X}}$ ). These relationships are predicted by the simple self-similar model of cluster formation, in which non-gravitational effects are ignored and the energy emission is dominated by thermal bremsstrahlung. The relations given by simulation and observation are different (Kravtsov et al. 2005; Nagai et al. 2007; Chen et al. 2007; Zhang et al. 2008),

---

Key Laboratory of Particle Astrophysics, Institute of High Energy Physics, Chinese Academy of Sciences, Beijing 100049; zhaohh@ihep.ac.cn

and these relations also vary with observable samples (Arnaud et al. 2007; Vikhlinin et al. 2009; Chen et al. 2007; Reichert et al. 2011).

Many simulations have shown that the slope of the  $M$ - $T$  relation was consistent with the self-similar value of 1.5 (Kravtsov et al. 2005; Nagai et al. 2007). Chen et al. (2007) also got the same result, using an isothermal model with *ROSAT* and *ASCA* data. Investigating 10 relaxed clusters observed by *XMM-Newton*, Arnaud et al. (2005) found that the slope of this relation was consistent with the expectation for hot clusters ( $T > 3.5$  keV), but was steeper for the whole sample. Sanderson et al. (2003) researched this relation using 66 clusters in the 0.5-15 keV temperature range. They derived a steeper slope of 1.84, and there was no obvious difference between the high mass and low mass parts. It is unclear whether the  $M$ - $T$  relation is consistent with the value expected by the self-similar model (Chen et al. 2007; Nagai et al. 2007); or this is true only for hot clusters (Arnaud et al. 2005); or the slope is steeper over the entire mass range (Sanderson et al. 2003).

Simulations and observations have shown that the  $M$ - $M_g$  relation was shallower than the self-similar prediction (Arnaud et al. 2005; Nagai et al. 2007). The discrepancy may be due to the dependence of gas fraction on the cluster mass. Zhang et al. (2008) obtained a slope of  $0.91 \pm 0.08$  for the  $M$ - $M_g$  relation using a sample of 37 LoCuSS clusters from *XMM-Newton* data. They also derived a steeper slope of  $0.97 \pm 0.08$ , which was consistent with the self-similar expectation, for the sub-sample of non-cool core clusters. The  $M$ - $M_g$  relation is very complicated. It is unclear whether the gas mass fraction depends on the mass (Vikhlinin et al. 2006; Giodini et al. 2009). There are also differences in the baryon fraction between cool-core systems and non-cool core systems (Eckert et al. 2012). The evolution of gas mass with cluster mass is not yet fully understood.

The  $L_X$ - $M$  relation is very important for the cosmological application. The  $L_X$ - $M$  relations differ significantly from different samples (Maughan 2007; Chen et al. 2007; Zhang et al. 2008; Pratt et al. 2009; Reichert et al. 2011). Reichert et al. (2011) obtained a slope of  $1.51 \pm 0.09$  by 14 literature samples. Using the core excised luminosity, Maughan et al. (2007) found that the slope was  $1.63 \pm 0.08$ . Chen et al. (2007) showed that the slope of  $1.94 \pm 0.15$  for the cool-core clusters (CCCs) agreed with that of  $1.75 \pm 0.25$  for the non-cool-core clusters (NCCCs) within errors. But there was a obvious difference in the normalizations of the relations for the CCCs and the NCCCs. Zhang et al. (2008) found that the slope ( $2.01 \pm 0.74$ ) for the NCCCs was shallower than that ( $2.32 \pm 0.70$ ) for the whole sample, while the errors were large.

$Y_X$ , the product of gas mass and X-ray temperature ( $Y_X = T \cdot M_g$ ), is another mass proxy. With the consideration of gas cooling and star formation, Kravtsov et al. (2006) found that the slope of the  $M$ - $Y_X$  relation was in good agreement with the self-similar prediction (Nagai et al. 2007). Arnaud et al. (2007) derived a slope of  $0.548 \pm 0.027$  with a sample of 10 relaxed clusters, which

was slightly shallower than the expected value.

Different cluster samples provide different results for the scaling relations (Arnaud et al. 2005; Chen et al. 2007; Nagai et al. 2007; Zhang et al. 2008; Reichert et al. 2011). It is necessary to build a large sample covering a wide range of temperature and including both CCCs and NCCCs observed by a telescope with high spatial resolution and sensitivity, such as *XMM-Newton* or *Chandra*. Moreover, a better method which can give more accurate X-ray parameters is also essential. To derive the cluster mass through so-called “scaling relations”, we should identify the best mass proxy. Ideally, a robust mass proxy should be characterized by that: (1) simple power law relation and evolution that can be close to the prediction of the self-similar model. (2) a low scatter in cluster mass. (3) stable relation does not vary with cluster sample. (4) cool cores have little influences on the relations.

Numerical simulations show that the  $Y_X$  may be a good mass indicator with only  $\approx 5\%$ - $8\%$  intrinsic scatter in  $M$  (Nagai et al. 2007; Kravtsov et al. 2006), which is smaller than any other mass proxies even in the presence of significant dynamical activity. Both simulations and observations show that the intrinsic scatter in mass around the  $M$ - $T$  relation is small ( $\Delta M/M \approx 0.10$ ) (Arnaud et al. 2005; Vikhlinin et al. 2006; Nagai et al. 2007). Arnaud et al. (2007) found that the scatter was the same for the  $M$ - $Y_X$  and  $M$ - $T$  relations. But the sample they used was small and only for relaxed clusters. They could not study whether the scatter was insensitive to dynamical state (Arnaud et al. 2007; Kravtsov et al. 2006). The  $M_g$  is also as a low-scatter proxy for  $M$  (Stanek et al. 2010; Okabe et al. 2010; Fabjan et al. 2011), this choice is motivated by the fact that  $M_g$  can be measured independent of the dynamical state of the cluster. Some authors showed that the scatter in the  $M$ - $M_g$  relation was smaller than that for the  $M$ - $Y_X$  relation (Okabe et al. 2010; Fabjan et al. 2011). For the hot and massive clusters, Mantz et al. (2010) found that the intrinsic scatter in the center-excised  $L_X$ - $M$  relation ( $<10\%$ ) was smaller than in either the  $M$ - $T$  or  $M$ - $Y_X$  relation (10-15%).

In this paper, we investigate a flux-limited sample of 39 X-ray nearby ( $z < 0.1$ ) galaxy clusters based on *XMM-Newton* observations. This sample covers a wide range of temperature (2-9 keV), and includes both CCCs and NCCCs. Using de-projecting method, we can derive accurate intra-cluster medium (ICM) temperature profiles and density distributions. The main goals of this work are: (1) to derive precise X-ray cluster parameters, e.g.,  $T$ ,  $L_X$ ,  $M$  and  $M_g$ , then to present four mass scaling relations:  $L_X$ - $M$ ,  $M$ - $T$ ,  $M$ - $M_g$  and  $M$ - $Y_X$ ; (2) to investigate the influences of cool core on the mass scaling relations; (3) to compare these scaling relations aiming to find which parameter is the best mass proxy. Throughout this paper, the energy band we select is 0.5-10 keV. We use a cosmological model with  $\Omega_M = 0.3$ ,  $\Omega_\Lambda = 0.7$  and  $H_0 = 70 \text{ km s}^{-1} \text{ Mpc}^{-1}$ . All uncertainties are in 68% confidence level.

## 2. Sample Selection

Using a flux-limited ( $f \geq 1.0 \times 10^{-11}$  erg s $^{-1}$  cm $^2$ ) method, we select a nearby ( $z < 0.1$ ) regular galaxy cluster sample from RASS (Grandi et al. 1999), HIFLUGCS (Thomas et al. 2002), REFLEX (Böhringer et al. 2004), NORAS (Böhringer et al. 2000), XBACs (Ebeling et al. 1996) and BCS (Ebeling et al. 1998) catalogs. Some clusters (e.g., A168, A2634, A3395), which are too weak to obtain their basic parameters, have been excluded from our sample. Because of the large angular size, we exclude the Coma, A3526, FORNAX, Perseus, Ophiuchus and Virgo clusters. Moreover, the clusters (e.g., A3562, A3266, A3667) with obvious substructures are unsuitable for detailed de-projected analysis and are excluded. At last, we select a sample of 39 clusters and all these clusters are available from *XMM-Newton* as listed in Table 1. This sample covers a broad temperature range of 2-9 keV.

To investigate the morphological characters of our sample, we calculate the values of centroid shift  $w$ , defined as the standard deviation between the X-ray surface brightness peak and the centroid of the system (Pratt et al. 2009):

$$\langle w \rangle = \left[ \frac{1}{N-1} \sum (\Delta_i - \langle \Delta \rangle)^2 \right]^{1/2} \times \frac{1}{r_{500}}, \quad (1)$$

We divide the 2D projected image into several concentric apertures centered on the X-ray surface brightness peak. The radii of apertures are  $n \times 0.05 \times r_{500}$  with  $n=4,5,6\dots 10$ , excluding the central regions to avoid bias associated with the bright central core. We obtain the centroid of each aperture by determining the “centre of mass” of the photon distribution.  $\Delta_i$  is the projected distance between the X-ray peak and the centroid in the  $i$ th aperture. The distribution of  $\langle w \rangle$  for our sample is shown in Fig.1, which shows that the upper limit of  $\langle w \rangle$  is 0.04. Compared to the upper limit value of 0.1 in Pratt et al. (2009), our sample have a more regular morphology.

## 3. Observations and Data Preparation

The basic data reduction is done with Science Analysis System (SAS) 11.2.0. In this paper, we consider the pn/EPIC data which are taken in Extended Full Frame mode or Full Frame mode. We only use the events with FLAG = 0, PATTERN  $\leq 4$ , the read out of time (OOT) effects are also corrected.

Since the X-ray flux of the cluster should be unchanged during the observation period, we discard all the intervals with prominent flares and then select only those intervals with count rates within  $3\sigma$  of the residual average count rate. The *XMM-Newton* background can approximately

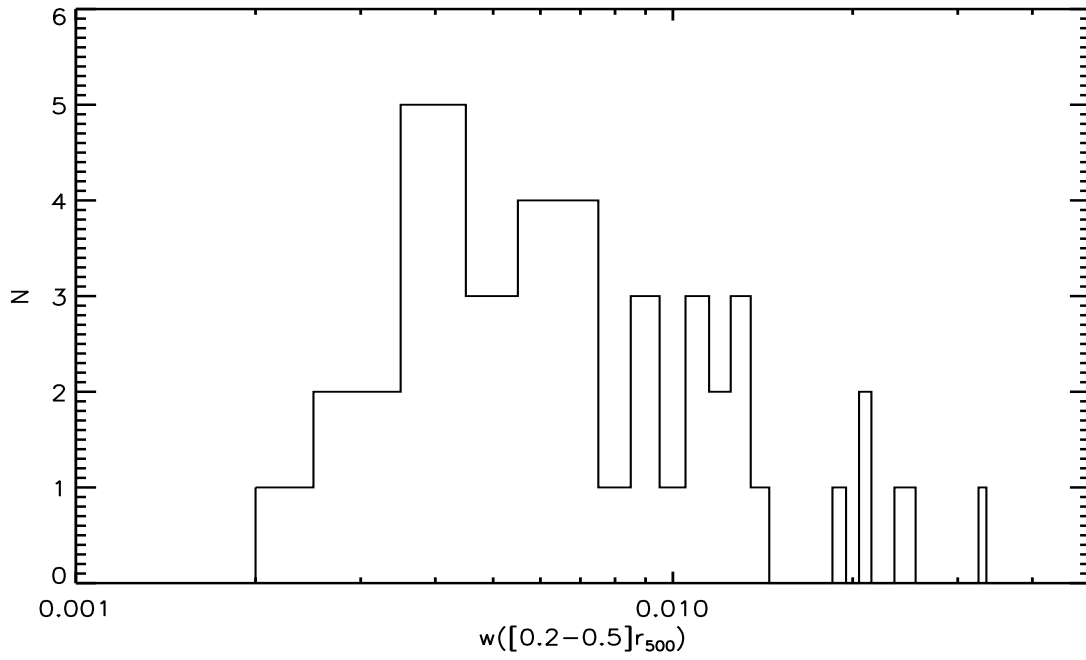


Fig. 1.— Histogram of central shift parameter  $\langle w \rangle$ , evaluated in the  $[0.2 - 0.5]r_{500}$  aperture.

be divided into two components. One is particle background, which dominates at high energy and has little or no vignetting. The other is Cosmic X-ray Background (CXB), which varies across the sky (Snowden et al. 1997), more important at low energies, and shows significant vignetting. We use the observations of ‘Lockman Hole’ (observation ID: 0147511801, hereafter LH) to subtract these two kinds of background. We estimate the ratio of the particle background between the cluster and LH from the total count rate in the region  $\theta \geq 10'$  in the high energy band (12-14 keV), as described in Pointecouteau et al. (2004). We use the outer flat region of the X-ray surface brightness distribution to monitor the residual background. At last, we apply a double-background subtraction method to correct for these two background components as used in Jia et al. (2004, 2006). The vignetting effects are also corrected.

All the galaxy clusters in this sample appear to be relaxed, therefore we assume the system structure to be spherically symmetric. We extract the spectra from annular regions centered on the X-ray emission peak. In order to ensure the signal to noise ratio, we use the criterion of  $\sim 2000$  net counts in 2-7 keV band per bin to determine the width of each ring (Zhang et al. 2006; Zhang et al. 2007). The minimum width of the rings is set at  $0.5'$ , which is wide enough for us to ignore the Point Spread Function (PSF) effect of *XMM-Newton* EPIC, whose Full Width at Half Maximum (FWHM) is  $6''$  for pn. Then, we can derive the de-projected spectra by subtracting all the contributions from the outer regions (see Jia et al. 2004, 2006 for detailed calculation).

## 4. X-Ray Properties

### 4.1. De-projected Temperature and Electron Density Profiles

The spectral analysis is carried out by using XSPEC version 12.6.0. We fit the de-projected spectra with the absorbed Mekeal model:

$$\text{Model} = \text{Wabs}(N_{\text{H}}) \times \text{Mekal}(T, z, A, \text{norm}), \quad (2)$$

in which Wabs is a photoelectric absorption model (Morrison & McCammon 1983), Mekal is a plasma emission model (Mewe et al. 1985; Kaastra 1992). The temperature  $T$ , metallicity  $A$  and  $\text{norm}$  (emission measure) are free parameters. The redshift  $z$  are fixed as in Table 1. For the majority of observations, the absorption  $N_{\text{H}}$  are fixed parameters, in a few case (i.e., A478, EXO 0422, Hercules),  $N_{\text{H}}$  are not unique, we left them as a free parameter. After obtaining the temperature of each shell, we can fit the radial de-projected temperature profile by the following equation (Xue et al. 2004):

$$T(r) = T_0 + \frac{A}{r/r_0} \exp\left(-\frac{(\ln r - \ln r_0)^2}{\omega}\right), \quad (3)$$

where  $T_0$ ,  $A$ ,  $r_0$ , and  $\omega$  are free parameters.

For calculating the de-projected electron density profile, we divide the cluster into several annular regions ( $> 14$ , depending on count rate of the cluster) centered on the emission peak. Then we use the de-projecting technique (see Jia et al. 2004, 2006 for detailed calculation) to calculate the photon counts in each shell. Since the de-projected temperature and abundance profiles are known, we can estimate the normalization ‘ $norm(i)$ ’ and its error in each shell. Then we can derive the de-projected electron density  $n_e$  of each region from Eq. (4).

$$norm(i) = \frac{10^{-14}}{4\pi[D(1+z)]^2} \int n_e n_H dV, \quad (4)$$

where  $D$  is the angular size distance to the source in cm. To obtain an acceptable fit for all clusters in this sample, we adopt a double- $\beta$  model to fit the electron density profile (Chen et al. 2003):

$$n_e(r) = n_{01} \left[ 1 + \left( \frac{r}{r_{c1}} \right)^2 \right]^{-\frac{3}{2}\beta_1} + n_{02} \left[ 1 + \left( \frac{r}{r_{c2}} \right)^2 \right]^{-\frac{3}{2}\beta_2}, \quad (5)$$

where  $n_{01}$  and  $n_{02}$  are electron number density parameters,  $\beta_1$  and  $\beta_2$  are the slope parameters, and  $r_{c1}$  and  $r_{c2}$  are the core radii of the inner and outer components, respectively.

The primary parameters of all 39 galaxy clusters are given in Table 1.

## 4.2. Mass Distribution

Once we have obtained the de-projected radial profiles of electron density  $n_e(r)$  and temperature  $T(r)$ , together with the assumptions of hydrostatic equilibrium and spherical symmetry, the gravitational mass of cluster within radius  $r$  can be determined as (Fabricant et al. 1980):

$$M(< r) = -\frac{k_B T r^2}{G \mu m_p} \left[ \frac{d(\ln n_e)}{dr} + \frac{d(\ln T)}{dr} \right], \quad (6)$$

where the mean molecular weight  $\mu$  is assumed to 0.62.  $k_B$ ,  $G$  and  $m_p$  are the Boltzman constant, the gravitational constant, and the proton mass, respectively. The mass of hot gas is calculated as:

$$M_g(< r) = 4\pi \mu_e m_p \int n_e(r) r^2 dr, \quad (7)$$

where  $\mu_e$  is the mean molecular weight of the electrons. We calculate the total mass and gas mass within  $r_{500}$ , in which the mean gravitational mass density is equal to 500 times the critical density at the cluster redshift. The total masses,  $M_{500}$ , and gas masses,  $M_g$ , within  $r_{500}$  for all the clusters are listed in Table 2.

### 4.3. Cooling Time

The cooling time  $t_{\text{cool}}$  is a timescale during which the hot gas loses all of its thermal energy. We calculate the cooling time of the gas as

$$t_{\text{cool}} = \frac{5}{2} \frac{n_e + n_i}{n_e} \frac{kT}{n_H \Lambda(A, T)}, \quad (8)$$

where  $\Lambda(A, T)$  is the cooling function of the gas and we fix the metallicity at  $A = 0.3Z_{\odot}$ .  $n_e$ ,  $n_H$ , and  $n_i$  are the number densities of the electrons, hydrogen, and ions, respectively. For the almost fully ionized plasma in clusters,  $n_e = 1.2n_H$  and  $n_i = 1.1n_H$ . The central cooling time  $t_c$  is derived from the central electron density  $n_{e0}$  and the central temperature  $T_0$ .  $n_{e0}$  is the electron density at  $r=0.004r_{500}$  (Hudson et al. 2010) and  $T_0$  is the average temperature within  $0-0.05r_{500}$ , where  $0.05r_{500}$  is the maximum value of the innermost annulus for the whole sample.

## 5. Partition of CCCs and NCCCs

Up to now, there are many methods used to distinguish CCCs from NCCCs, but it is unsure which is the best. CCCs is defined differently often based on a significant central temperature drop (Sanderson et al. 2006; Arnaud et al. 2007; Burn et al. 2008), short central cooling time (Bauer et al. 2005; O’Hara et al. 2006; Donahue 2007), significant classical mass deposition rate (Chen et al. 2007) or low central entropy (Hudson et al. 2010). Hudson et al. (2010) found that central cooling time was the best parameter for low redshift clusters, and that cuspsiness (defined as  $\alpha = -\frac{d\log(n)}{d\log(r)}$ ) was the best parameter for high redshift cluster.

We define CCCs by two criteria, (1) the central cooling time,  $t_c$ , is shorter than  $7.7h_{70}^{-1/2}$  Gyr (Rafferty et al. 2006); (2) there is an obvious temperature drop compared with the peak temperature ( $> 30\%$ ) towards the cluster center. Using this two criteria, we divide our sample into NCCCs and CCCs, the fractions are 36% and 64%, respectively.

The central entropy,  $K_0$  ( $K_0 = kT_0n_{e0}^{-2/3}$ ), is another parameter to distinguish CCCs from NCCCs (Hudson et al. 2010). The  $K_0$  can divide a sample at  $\sim 22$  and  $\sim 150 h_{70}^{-1/3}$  keV cm<sup>2</sup>, for the strong cool-core cluster (SCCC), weak cool-core cluster (WCCC), and NCCC (Hudson et al. 2010), respectively.  $t_c$  can also divide a sample at  $1.0 h_{70}^{-1/2}$  Gyr and  $7.7 h_{70}^{-1/2}$  Gyr (Vikhlinin et al. 2007; Hudson et al. 2010). In Fig.2, we compare the difference in sorting the sample using  $K_0$  or  $t_c$ . Combining  $K_0$  and  $t_c$ , the dash lines show the division between SCCC and WCCC, the dash-dot lines show the division between WCCC and NCCC. The filled circles represent the pronounced CCCs, and the open triangles show NCCCs. Based on Fig.2, there is no much difference in sorting the sample using  $K_0$  or  $t_c$ . With our definition of the CCC, we divide the WCCCs into CCCs and NCCCs.



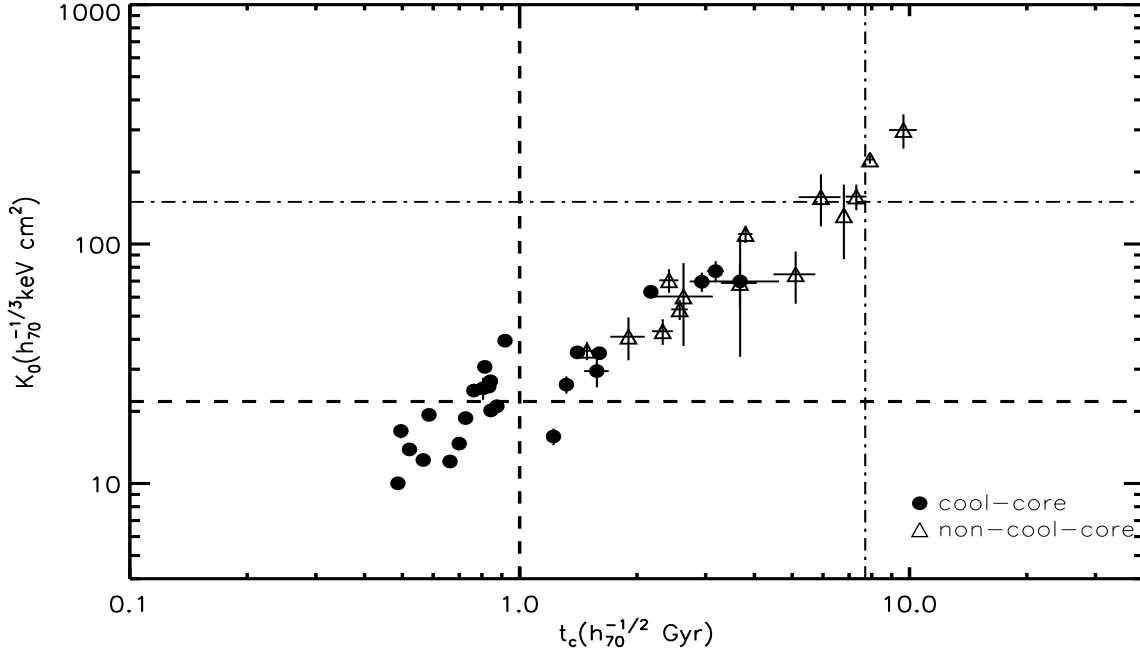


Fig. 2.— This plot shows central entropy ( $K_0$ ) versus central cooling time  $t_c$ . The  $K_0$  can divide a sample at  $\sim 22$  and  $\sim 150 h_{70}^{-1/3} \text{ keV cm}^2$ , for the strong cool-core cluster (SCCC), weak cool-core cluster (WCCC), and NCCC (Hudson et al. 2010), respectively.  $t_c$  can also divide a sample at  $1.0 h_{70}^{-1/2} \text{ Gyr}$  and  $7.7 h_{70}^{-1/2} \text{ Gyr}$  (Vikhlinin et al. 2007; Hudson et al. 2010). Combining  $K_0$  and  $t_c$ , the dash lines show the division between SCCC and WCCC, the dash-dot lines show the division between WCCC and NCCC. The filled circles represent the pronounced CCCs, and the open triangles show NCCCs.

## 6. Self-similarity of the Scaled Profiles of the X-Ray Properties

### 6.1. Scaled Temperature Profiles

We derive the global temperature,  $T_{(0.2-0.5)r_{500}}$ , by the volume average of the radial temperature profile limited to the radial range of  $(0.2-0.5)r_{500}$ , as listed in Table 1. The temperatures within  $0.2r_{500}$  tend to show peculiarities linked to the cluster dynamical history, which are mainly affected by the cool cores (Smith et al. 2005). The upper boundary of  $0.5r_{500}$  is limited by the quality of the spectral data. Thus, using temperature within  $(0.2-0.5)r_{500}$ , we can minimize the scatter in the X-ray scaling relations and reach a better agreement between the X-ray scaling relations for the CCCs and NCCCs. Fig.3 shows the temperature profiles for the CCC sub-sample and the NCCC sub-sample, respectively. There is a special cluster (Hercules), which has a rapid fluctuation in the temperature profile for the CCC sub-sample, and the unique distribution is also confirmed by the *Chandra* data (Cavagnolo et al. 2009; Li et al. 2013).

### 6.2. X-ray Scaling Relations

In the following, we investigate the relationships between several parameters. We perform the relations with logarithmic values of the parameters in the form:

$$\log_{10}(Y) = A + B \cdot \log_{10}(X), \quad (9)$$

where  $X$  and  $Y$  represent the variables,  $A$  and  $B$  are the two free parameters to be estimated. We firstly create the histogram of residuals from the best fitting relation in the log space, and then, the raw scatter can be obtained by a Gaussian fitting to the histogram. The intrinsic scatter is calculated as (Morandi et al. 2007):

$$S = \left[ \sum_j \left( (\log_{10}(Y_j) - A - B \log_{10}(X_j))^2 - \epsilon_{\log_{10}(Y_j)}^2 \right) / (N - 2) \right]^{1/2}, \quad (10)$$

where  $\epsilon_{\log_{10}(Y_j)} = \epsilon_{Y_j} / (Y_j \ln 10)$ , with  $\epsilon_{Y_j}$  being the statistical error of the measurement  $Y_j$ , and  $N$  is the total number of data.

### 6.3. The $M_{500}$ - $T$ Relation

It is well known that different regression methods may give different slopes even at the same population level (Akritas & Bershadsky 1996). Therefore, it is important to choose the most suitable

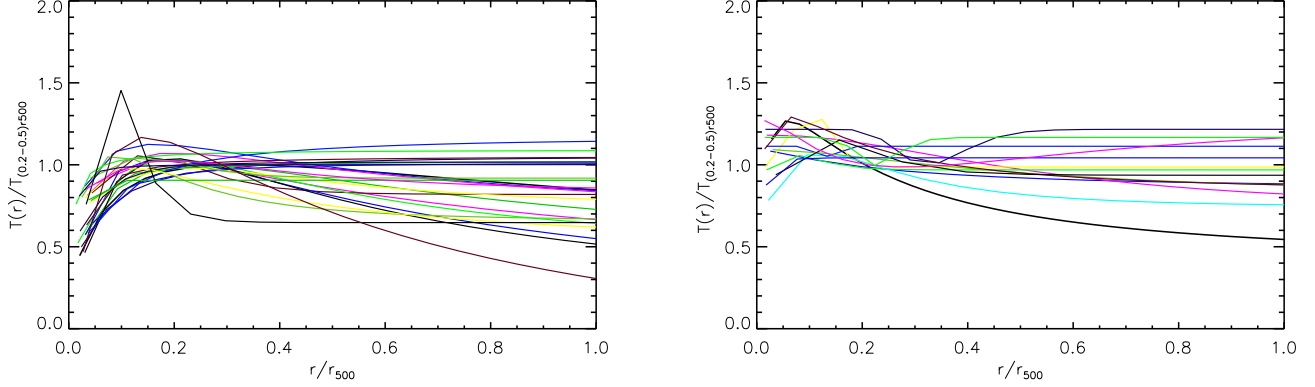


Fig. 3.— Temperature profiles. Left panel: The temperature profiles for the CCC sub-sample. Right panel: The temperature profiles for the NCCC sub-sample. We scale the temperature profiles by  $T_{(0.2-0.5)r_{500}}$  and  $r_{500}$ .

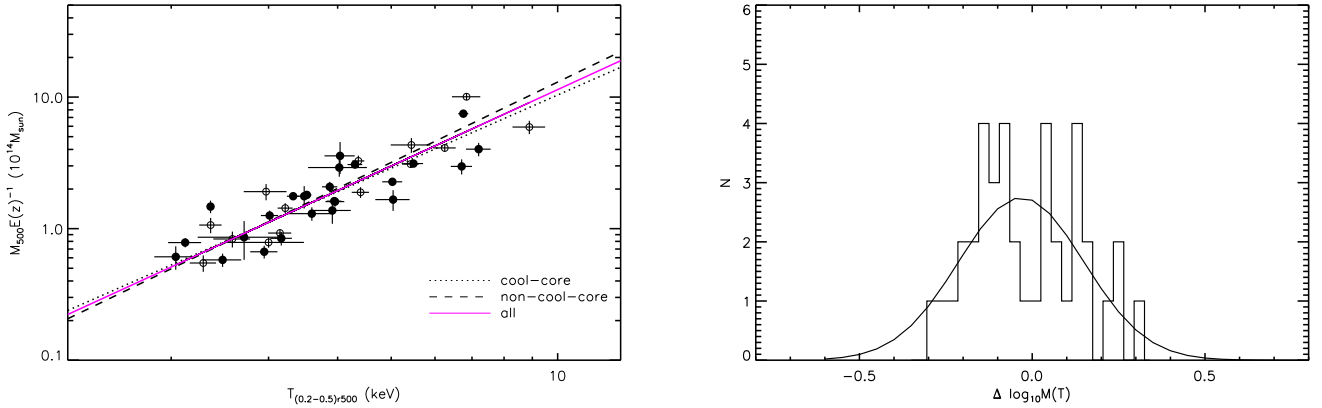


Fig. 4.— Left panel: Total mass versus temperature diagram. In the following, the filled circles and open circles represent the CCCs and NCCCs, respectively;  $E^2(z) = \Omega_m(1+z)^3 + \Omega_\Lambda$  describes the evolution of the Hubble constant for a flat universe; The red solid line shows the fit for all the data and the dashed and dotted lines are those for the NCCCs and CCCs, respectively. Right panel: Histogram of the residuals from the  $M_{500}$ - $T$  relation in log space. This raw scatter is well described by a Gaussian fit of  $\sigma_{M(T)} = 0.18$  dex.

method for different data. In  $M_{500}-T$  relation, we compare four kinds of BCES regression methods (BCES(Y|X), BCES(X|Y), BCES Bisector, BCES Orthogonal), all of which take into account both intrinsic scatter and the presence of errors on both variables (Akritas & Bershady 1996). The best power-law fits given by these four methods are shown in Table 3. The slopes from these four methods are consistent within  $1\sigma$  errors. In order to compare with previous results, we use the BCES Bisector method. The results of power-law fits in the BCES Bisector method for all the relations discussed in section 6 are summarized in Table 4.

Fig.4 shows the  $M_{500}-T$  relation for our sample. Considering the whole sample, our best-fit slope  $1.94 \pm 0.17$  is higher than the self-similar predictive value, 1.5. The slope is consistent with the result in Mantz et al. (2010),  $2.08 \pm 0.08$  for a 238 galaxy cluster sample observed by *Chandra* or *ROSAT*. Reichert et al. (2011) derived a slope of  $1.76 \pm 0.08$  from the 14 literature samples. Our slope is also consistent with the result of Sanderson et al. (2003),  $1.84 \pm 0.01$  for the  $M_{200}-T$  relation using *ASCA* temperature profiles. Previous studies have suggested that the slopes of the  $M_{200}-T$  relation for the high mass and low mass parts may be different (Finoguenov et al. 2001; Dos Santos 2007). The cross-over temperature between the two parts is typically  $\sim 3.0$  keV (Finoguenov et al. 2001). Sanderson et al. (2003) investigated a sample, which included 66 clusters with a broad range of temperature (0.5-15 keV), and found no obvious break in the  $M_{200}-T$  relation at  $\sim 3.0$  keV. We also obtain a similar slope of  $1.99 \pm 0.30$  for a sub-sample with  $T > 3.0$  keV from our sample. Thus, our slope is steeper than the self-similar prediction, and it does not vary with the temperature (or mass) range of the sample.

Fixing the slope to 2.08, we find that the normalization of our relation is lower by  $\sim 28\%$  than that in Mantz et al. (2010). With the slope fixed to 1.76, the normalization for our sample is lower than that in Reichert et al. (2011) by  $\sim 27\%$ .

Moreover, the slopes and the normalizations of the  $M_{500}-T$  relation for the CCCs and NCCCs are consistent within errors as listed in Table 4. This indicates that no evident influence of cool core is found on this relation. This agrees with the result obtained by Chen et al. (2007), who considered a 88 cluster sample based on *ASCA* and *ROSAT* observations.

The right panel of Fig.4 shows a histogram of the log space residuals from the best fitting  $M_{500}-T$  relation for the whole sample. The residuals are corresponding to the value of vertical distances to the best fitting line (Pratt et al. 2009). The raw scatter of the  $M_{500}-T$  relation is well described by a Gaussian fit in log space with  $\sigma_{M(T)} = 0.18$  dex. The intrinsic scatter in  $M_{500}$  around the  $M_{500}-T$  relation is 0.14 dex.

#### 6.4. The $M_{500}$ - $M_g$ Relation

Fig.5 shows the  $M_{500}$ - $M_g$  relation for our sample and the best-fit gives a slope of  $0.79 \pm 0.07$ . The slope is in agreement with  $0.81 \pm 0.07$  derived from *Chandra* data (Kravtsov et al. 2006; Nagai et al. 2007) and in marginal agreement with  $0.91 \pm 0.08$  presented by Zhang et al. (2008). The slope is shallower than the self-similar prediction ( $M_{500} \propto f_g^{-1} M_g$ ). This may be due to the trend of observed  $f_g$  with the total mass. Giodini et al. (2009) investigated a sample of 41 clusters, which spanned the total mass range  $1.5 \times 10^{13} M_\odot$ - $1.1 \times 10^{15} M_\odot$ , and found  $f_g \propto M^{0.21}$ . Taking this trend into account, the slope of the  $M_{500}$ - $M_g$  relation is about 0.79, which is in good agreement with our result. The normalization of our  $M_{500}$ - $M_g$  relation is lower by  $\sim 24\%$  using a fixed slope of 0.91, and higher by 9% with the slope fixed to 0.81 for the *Chandra* data. The slopes of the  $M_{500}$ - $M_g$  for the CCCs and NCCCs are consistent within errors. The influence of cool core is not found on this relation.

The right panel in Fig.5 shows a histogram of the log space residuals from the  $M_{500}$ - $M_g$  relation for the whole sample. This raw scatter is well described by a Gaussian fit in log space with  $\sigma_{M(M_g)} = 0.14$  dex. The intrinsic scatter in  $M_{500}$  around the  $M_{500}$ - $M_g$  relation is 0.14 dex.

#### 6.5. The $L_{\text{bol}}$ - $M_{500}$ Relation

The  $L_{\text{bol}}$ - $M_{500}$  relation is very important for the application to cosmological cluster surveys. Fig.6 shows the  $L_{\text{bol}}$ - $M_{500}$  relation for our sample and the best fit gives a slope of  $1.73 \pm 0.16$ . Our slope is higher than the self-similar expected value, 1.33, and agrees with the results obtained by Reiprich & Böhringer (2002) ( $1.80 \pm 0.08$ ) and Ettori et al. (2004) ( $1.88 \pm 0.42$ ), in both of which the same core-uncorrected  $L_{\text{bol}}$  are used as ours. Our slope is lower than the core-corrected result of Zhang et al. (2008,  $2.36 \pm 0.07$ ). The slope of our relation is consistent with the result of Morandi et al. (2007,  $2.00 \pm 0.28$ ), in which the  $L_{\text{bol}}$  was obtained by excluding the  $r < 100$  kpc region.

The slope for the NCCCs ( $1.38 \pm 0.17$ ) is consistent with the self-similar expected value, while the slope ( $2.03 \pm 0.22$ ) for the CCCs is higher. There is a significant normalization discrepancy between CCCs and NCCCs. These may be due to the high luminosity of the cool core in CCCs.

The right panel in Fig.6 shows a histogram of the log space residuals from the  $L_{\text{bol}}$ - $M_{500}$  relation for the whole sample. This raw scatter in  $M_{500}$  is well described by a Gaussian fit in log space with  $\sigma_{M(L_{\text{bol}})} = 0.27$  dex. The intrinsic scatter in  $M_{500}$  around the  $L_{\text{bol}}$ - $M_{500}$  relation is 0.15 dex.

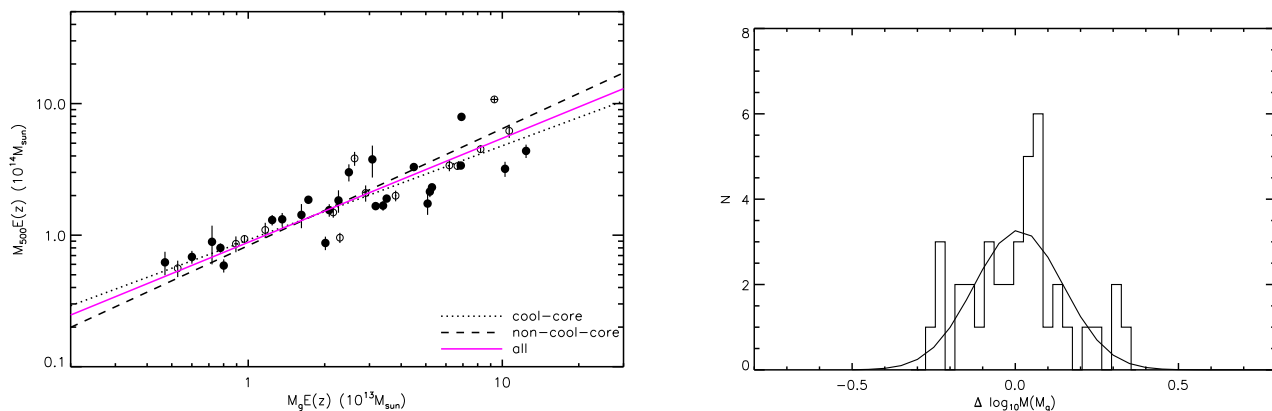


Fig. 5.— Left panel: The total mass versus gas mass inside  $r_{500}$ . Right panel: Histogram of the residuals from the  $M_{500}$ - $M_g$  relation in log space. This raw scatter is well described by a Gaussian fit of  $\sigma_{M(M_g)} = 0.14$  dex.

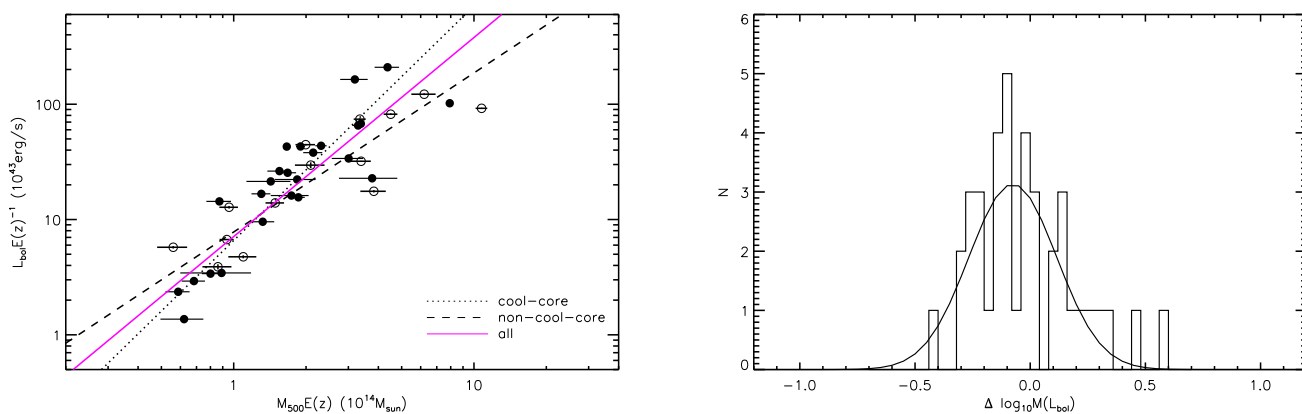


Fig. 6.— Left panel: X-ray luminosity in the 0.01-100 keV band versus the total mass. Right panel: Histogram of the residuals from the  $M_{500} - L_{bol}$  relation in log space. This raw scatter is well described by a Gaussian fit of  $\sigma_{M(L_{bol})} = 0.27$  dex.

## 6.6. The $M_{500}$ - $Y_X$ Relation

We present the  $M_{500}$ - $Y_X$  relation for this sample in Fig.7, in which the best-fit gives a slope of  $0.57 \pm 0.04$  being consistent with 0.6 expected by the self-similar model. Our slope is consistent with the result of  $0.62 \pm 0.06$  in Zhang et al. (2008), who used the same temperature,  $T_{(0.2-0.5)r_{500}}$ , as ours. The slope is also in good agreement with the value  $0.57 \pm 0.03$  in Vikhlinin et al. (2009), in which a extended temperature was used in the radial range  $(0.15-1)r_{500}$  for ten relaxed *Chandra* clusters. Moreover, our result is supported by the simulation ( $0.57 \pm 0.01$ ) (Nagai et al. 2007). Thus, the slope of  $M_{500}$ - $Y_X$  relation is stable and not sensitive to the temperature definition.

The right panel in Fig.7 shows a histogram of the log space residuals from the  $M_{500}$ - $Y_X$  relation for all clusters. This raw scatter in  $M_{500}$  is well described by a Gaussian fit in log space with  $\sigma_{M(Y_X)} = 0.13$ , which is the smallest among the relation between the observables and the total mass. We also obtain a small intrinsic scatter of 0.13 dex. Fixing the slope to 0.62, we find that the normalization of our relation is lower than that in Zhang et al. (2008) by  $\sim 19\%$ . We also fix the slope to 0.57, and find that the normalization of our slope is similar with the simulation value by  $\sim 2\%$ .

The slope for the relation of the NCCCs agrees with that for the CCCs within errors as listed in Table 4. Both slopes are close to the self-similar prediction (0.6). Taking the errors into account, the normalization for the NCCCs is also consistent with that for the CCCs.

## 7. Discussion

### 7.1. Comparison of Different Mass-Proxy Relations

In this section, we compare the four mass scaling relations ( $L_{\text{bol}}-M_{500}$ ,  $M_{500}-T$ ,  $M_{500}-M_g$  and  $M_{500}-Y_X$ ), to find out which relation is the best to estimate cluster mass. The comparison of these relations are listed in Table 5.

The slope of the  $L_{\text{bol}}-M_{500}$  relation ( $1.73 \pm 0.16$ ) is steeper than the self-similar expectation (1.33) significantly. It may be due to that the  $L_{\text{bol}}$  is dominated by cluster center and thus particularly susceptible to nongravitational processes, while the self-similarity is roughly preserved in the outer region. For the  $M_{500}-T$  relation, we perform the fittings for both the hot clusters ( $T > 3.0$  keV) and the whole sample, and find that the slopes are steeper than the self-similar value and do not vary with the cluster temperature range. The slope of the  $M_{500}-M_g$  relation is shallower than the self-similar prediction, moreover, the gas fraction seems to depend on the  $M_{500}$  rather than a constant. The  $M_{500}-Y_X$  relation agrees with the self-similarity and is consistent with the simulations (Kravtsov et al. 2005; Nagai et al. 2007).

Both intrinsic scatters and raw scatters show that the  $M_{500}-Y_X$  relation is the tightest one compared with the  $M_{500}-T$ ,  $M_{500}-M_g$  and  $L_{\text{bol}}-M_{500}$  relations. Numerical simulations also indicate that the  $Y_X$  is a low-scatter mass proxy (with only  $\approx 5\%-8\%$  intrinsic scatter) (Nagai et al. 2007; Kravtsov et al. 2006), which is smaller than any other mass proxies even in the presence of significant dynamical activity.

The  $L_{\text{bol}}-M_{500}$  relation has the largest discrepancy in the slopes between CCCs ( $2.03 \pm 0.22$ ) and NCCCs ( $1.38 \pm 0.17$ ), indicating a significant influence of the cool core on this relation. The slope for the NCCCs is consistent with the self-similar expected, while the slope for the CCCs is steeper (Table 3). In contrast, the slopes of the other relations display much smaller differences between CCCs and NCCCs. That indicates the cool core has little influence on the  $M_{500}-T$ ,  $M_{500}-M_g$  and  $M_{500}-Y_X$  relations.

Many large cluster samples have been used to investigate the scaling relations. We compare recent results in Table 6. Both simulations (Nagai et al. 2007, Fabjan et al. 2011) and observations (Arnaud et al. 2007, Vikhlinin et al. 2009, Li et al. 2013) show that the relation of  $M_{500}-Y_X$  is in good agreement with the self-similar expected value, 0.6, and does not change with cluster sample, while the other relations are quite different between samples. Compared to the other relations, the  $M_{500}-Y_X$  relation is the most insensitive to variations in the physical processes included in the simulation (Poole et al. 2007; Rasia et al. 2011; Fabjan et al. 2011).

In sum, the  $M_{500}-Y_X$  relation is the stablest one among these four scaling relations, which is in agreement with the self-similar model and does not changes with the cluster sample. In addition, this relation has the smallest scatter in  $M_{500}$  and does not affected by the cool core. Thus, the parameter  $Y_X$  is the best proxy to estimate cluster mass.

## 7.2. Correction for Malmquist bias

For X-ray flux-limited cluster samples, more luminous clusters will be selected from a survey volume and this will induce the Malmquist bias. Many works have pointed out that the observed  $L_X-M$  scaling relation may be significantly affected by Malmquist bias if the scatter in luminosity for fixed mass is large (Stanek et al. 2006; Vikhlinin et al. 2009; Pratt et al. 2009). We can give the mean bias in  $\ln L$  for given mass (Vikhlinin et al. 2009):

$$Bias(\ln L | \ln L_0) = \langle \ln L \rangle - \ln L_0 = \frac{\int_{-\infty}^{\infty} (\ln L - \ln L_0) p(\ln L) V(\ln L) d \ln L}{\int_{-\infty}^{\infty} p(\ln L) V(\ln L) d \ln L} \quad (11)$$

where  $\ln L_0$  is the mean  $L$  for given mass, and  $p(\ln L)$  has a log-normal distribution ( $p(\ln L) \propto -(\ln L - \ln L_0)^2 / (2\sigma^2)$ ), which characterizes the scatter of  $L$  in the  $L_X-M$  relation. For the low



redshift and flux-limited sample, the evolution on the  $L_X$ - $M$  relation can be neglected within the survey's effective redshift depth (Vikhlinin et al. 2009), and the survey volume is a power law function of the object luminosity ( $V(L) \propto L^{3/2}$  in Euclidean space). Thus, the Eq. (11) can be worked out analytically with  $Bias(\ln L | \ln L_0) = 3/2\sigma^2$ . We also perform a Gaussian fitting for the  $L_{bol}$ - $M_{500}$  relation and find  $\sigma=0.65$ , the bias is 0.63. Thus, the Malmquist bias leads to a 87% overestimation in the normalization of the observed  $L_{bol}$ - $M_{500}$  relation in our sample, which is much smaller than the factor of 2 bias advocated by Stanek et al. (2006) but larger than the value 26% in Vikhlinin et al. (2009).

### 7.3. Uncertainties in the measurement of cluster mass

The total cluster mass may be affected by some factors. First, the assumption of spherical symmetry is not satisfied in some clusters, thus, the masses of these clusters may be overestimated (or underestimated). To estimate the uncertainty due to spherical symmetry, Landry et al. (2012) found a  $\pm 6\%$  systematic uncertainty in the total mass of the most disturbed clusters, A520, at  $r_{500}$ . All the clusters in our sample are regular and round in projected image, but in case of merging along the line-of-sight, the inaccuracy may be large due to the assumption of spherical symmetry. Second, all the clusters in our sample are nearby, at redshift  $z < 0.1$ . The temperature profiles to  $r_{500}$  are unavailable for some clusters. In this case, we use the extended temperature profile to calculate the cluster mass, which will introduce some errors. We select a NCCC (A3391) and a CCC (A1650), whose temperatures at  $r_{500}$  are available, to test the uncertainties due to the possibility of mis-extrapolating the temperature profile. We fit the temperature profiles without the outmost observed data, and then obtain their cluster masses again. Compared with the previous masses, the biases in the cluster mass due to the mis-extrapolating temperature profiles for A1650 and A3391 are 17% and 4%, respectively. Third, the hydrostatic equilibrium may be destroyed and non-thermal pressure components become more significant at large radius (Nagai et al. 2007; Zhang et al. 2008; Vikhlinin et al. 2009). The subsonic turbulent motions of the ICM gas in relaxed clusters in the Nagai et al. (2007) sample seem to result in a  $\sim 15\%$  underestimate in the hydrostatic estimates of  $M_{500}$ .

## 8. Conclusion

Using a sample of 39 X-ray nearby ( $z < 0.1$ ) galaxy clusters observed with *XMM-Newton*, we investigate the relations between X-ray observables and total mass. The observable parameters (e.g.  $L_{bol}$ ,  $T$ ,  $M_g$  and  $M_{500}$ ) are precisely derived by de-projecting technique. With the criterion of the central cooling time and the central temperature, we divide the clusters in this sample into

NCCCs and CCCs and the fractions are 36% and 64%, respectively. Furthermore, we study the scaling relations of  $L_{\text{bol}}-M_{500}$ ,  $M_{500}-T$ ,  $M_{500}-M_{\text{g}}$  and  $M_{500}-Y_{\text{X}}$ , and also the influences of cool core on these relations. The results show that the  $M_{500}-Y_{\text{X}}$  relation has a slope close to the standard self-similar value, has the smallest scatter and does not vary with the cluster sample. Moreover, the  $M_{500}-Y_{\text{X}}$  relation is not affected by the cool core. Thus, the parameter of  $Y_{\text{X}}$  may be the best mass indicator.

This research was supported by the National Natural Science Foundation of China under grant Nos. 11003018, 11203019, and by the Strategic Priority Research Program on Space Science, the Chinese Academy of Sciences, Grant No. XDA04010300.

## REFERENCES

- Akritas, M. G., & Bershadsky, M. A. 1996, *ApJ*, 470, 706
- Arnaud, M., Pointecouteau, E., & Pratt, G. W. 2005, *A&A*, 441, 893
- Arnaud, M., Pointecouteau, E., & Pratt, G. W. 2007, *A&A*, 474, L37
- Bauer, F. E., Fabian, A. C., Sanders, J. S., et al. 2005, *MNRAS*, 359, 1481
- Böhringer, H., Schuecker, P., Guzzo, L., et al. 2004, *A&A*, 425, 367
- Böhringer, H., Voges, W., Huchra, J. P., et al. 2000, *ApJ*, 129, 435
- Burn, J. O., Hallman, E.J., Gantner, B., et al. 2008, *ApJ*, 675, 1125
- Cavagnolo, K. W., Donahue, M., Voit, G. M., Sun, M. 2009, *ApJ*, 182, 12
- Chen, Y., Ikebe, Y. & Böhringer, H. 2003, *A&A*, 407, 41
- Chen, Y., Reiprich, T. H., Böhringer, H., et al. 2007, *A&A*, 466, 805
- Donahue, M., 2007, in *Heating versus Cooling in Galaxies and Clusters of Galaxies*, EOS Astrophysics Symposia, ed. H. Böhringer, G. W. Pratt, A. Finoguenov, & P. Schuecker (Heidelberg, Berlin: Springer-verlag), 20
- Dos Santos, S., Dorë, O., 2002, *A&A*, 383, 450
- Ebeling, H., Voges, W., Böhringer, H., et al. 1996, *MNRAS*, 281, 799
- Ebeling, H., Edge, A. C., Bohringer, H., et al. 1998, *MNRAS*, 301, 881

Table 1: *XMM-Newton* observations and cluster properties.

Cluster	OBS-ID	$z$	$N_{\text{H}}$ $10^{20}\text{cm}^{-2}$	$T_{(0.2-0.5)r_{500}}$ keV	$L_{0.1-2.4\text{keV}}$ $10^{44}\text{erg/s}$	$L_{0.01-100\text{keV}}$ $10^{44}\text{erg/s}$
2A0335	0109870101	0.0347	18.6	$4.03 \pm 0.80$	$2.10 \pm 0.04$	$3.44 \pm 0.07$
A0133	0144310101	0.0569	1.6	$4.04 \pm 0.42$	$1.40 \pm 0.02$	$2.34 \pm 0.06$
A1650	0093200101	0.0845	1.5	$5.49 \pm 0.37$	$3.55 \pm 0.03$	$7.05 \pm 0.09$
A1795	0097820101	0.0622	1.2	$6.75 \pm 0.23$	$5.26 \pm 0.02$	$10.49 \pm 0.08$
A2029	0111270201	0.0766	3.2	$6.70 \pm 0.48$	$7.70 \pm 0.08$	$17.01 \pm 0.25$
A2052	0401521201	0.0353	2.9	$3.16 \pm 0.23$	$0.93 \pm 0.01$	$1.46 \pm 0.02$
A2065	0202080201	0.0723	2.8	$5.02 \pm 0.34$	$2.14 \pm 0.03$	$4.40 \pm 0.13$
A2199	0008030201	0.0299	0.8	$3.98 \pm 0.19$	$2.47 \pm 0.01$	$4.35 \pm 0.03$
A0262	0109980101	0.0163	5.5	$2.48 \pm 0.33$	$0.16 \pm 0.01$	$0.24 \pm 0.01$
A2626	0148310101	0.0565	4.3	$3.32 \pm 0.14$	$1.03 \pm 0.01$	$1.60 \pm 0.03$
A2657	0505210301	0.0404	5.3	$3.91 \pm 0.51$	$1.28 \pm 0.06$	$2.18 \pm 0.21$
A3112	0105660101	0.0752	2.5	$4.30 \pm 0.21$	$3.83 \pm 0.03$	$6.77 \pm 0.08$
A3558	0107260101	0.0488	3.6	$5.04 \pm 0.59$	$0.82 \pm 0.01$	$1.65 \pm 0.04$
A3581	0205990101	0.023	4.3	$2.12 \pm 0.24$	$0.26 \pm 0.01$	$0.34 \pm 0.01$
A4059	0109950201	0.0475	1.1	$3.96 \pm 0.25$	$1.49 \pm 0.01$	$2.60 \pm 0.03$
A0478	0109880101	0.0882	15.3	$7.20 \pm 0.60$	$10.32 \pm 0.11$	$21.84 \pm 0.17$
A0496	0506260401	0.0326	5.7	$3.87 \pm 0.20$	$2.33 \pm 0.02$	$3.86 \pm 0.04$
S1101	0123900101	0.0564	1.9	$2.36 \pm 0.06$	$1.93 \pm 0.01$	$2.70 \pm 0.02$
AWM 7	0135950301	0.0172	9.21	$3.59 \pm 0.57$	$0.52 \pm 0.01$	$0.96 \pm 0.10$
EXO0422	0300210401	0.0390	6.4	$3.01 \pm 0.18$	$1.00 \pm 0.02$	$1.70 \pm 0.02$
Hercules	0401730101	0.0370	3.4	$2.70 \pm 0.78$	$0.22 \pm 0.01$	$0.35 \pm 0.01$
HydraA	0504260101	0.0538	4.86	$3.52 \pm 0.11$	$2.74 \pm 0.01$	$4.41 \pm 0.03$
MKW3S	0109930101	0.0442	3.2	$3.48 \pm 0.15$	$1.38 \pm 0.01$	$2.27 \pm 0.03$
MKW4	0093060101	0.0195	1.9	$2.04 \pm 0.29$	$0.10 \pm 0.01$	$0.14 \pm 0.01$
MKW8	0300210701	0.0263	2.6	$2.95 \pm 0.27$	$0.19 \pm 0.01$	$0.30 \pm 0.01$
A1060	0206230101	0.0126	4.9	$3.15 \pm 0.25$	$0.41 \pm 0.01$	$0.67 \pm 0.01$
A1651	0203020101	0.0845	1.7	$5.42 \pm 0.31$	$3.94 \pm 0.07$	$7.72 \pm 0.19$
A2063	0200120401	0.0358	2.9	$3.00 \pm 0.78$	$0.89 \pm 0.03$	$1.41 \pm 0.06$
A2589	0204180101	0.0416	4.39	$3.22 \pm 0.16$	$0.88 \pm 0.01$	$1.42 \pm 0.03$
A3158	0300210201	0.0590	1.1	$4.40 \pm 0.18$	$2.46 \pm 0.04$	$4.58 \pm 0.12$
A3391	0505210401	0.0514	5.4	$5.44 \pm 0.74$	$0.92 \pm 0.02$	$1.80 \pm 0.07$
A3571	0086950201	0.0391	3.9	$4.36 \pm 0.18$	$1.73 \pm 0.02$	$3.26 \pm 0.04$
A3827	0406200101	0.098	2.8	$6.24 \pm 0.48$	$4.71 \pm 0.06$	$8.58 \pm 0.23$
A0399	0112260301	0.0722	10.6	$6.84 \pm 0.66$	$4.13 \pm 0.05$	$9.53 \pm 0.17$
A0400	0404010101	0.0238	8.9	$2.29 \pm 0.21$	$0.44 \pm 0.02$	$0.58 \pm 0.02$
A4010	0404520501	0.0957	1.4	$2.96 \pm 0.43$	$2.01 \pm 0.07$	$3.10 \pm 0.29$
AWM 4	0093060401	0.0326	4.8	$2.58 \pm 0.32$	$0.25 \pm 0.01$	$0.40 \pm 0.03$
Triangulum	0093620101	0.051	5.4	$8.89 \pm 0.99$	$4.83 \pm 0.12$	$12.48 \pm 0.36$
IIIZw54	0505230401	0.0311	16.68	$2.36 \pm 0.18$	$0.32 \pm 0.01$	$0.48 \pm 0.02$

Table 2: *XMM-Newton* observations and cluster properties.

Cluster	$r_{500}$ Mpc	$t_c$ Gyr	$M_{\text{tot},500}$ $10^{14}M_{\odot}$	$M_g$ $10^{13}M_{\odot}$	cc*
2A0335	$0.93 \pm 0.01$	$0.52 \pm 0.01$	$2.96 \pm 0.44$	$2.45 \pm 0.01$	Y
A0133	$1.07 \pm 0.10$	$0.87 \pm 0.01$	$3.67 \pm 1.00$	$3.01 \pm 0.03$	Y
A1650	$1.02 \pm 0.01$	$2.17 \pm 0.07$	$3.25 \pm 0.13$	$6.60 \pm 0.01$	Y
A1795	$1.39 \pm 0.01$	$0.84 \pm 0.01$	$7.70 \pm 0.18$	$6.71 \pm 0.15$	Y
A2029	$1.00 \pm 0.04$	$0.91 \pm 0.02$	$3.08 \pm 0.40$	$9.89 \pm 0.04$	Y
A2052	$0.66 \pm 0.03$	$0.70 \pm 0.01$	$0.86 \pm 0.01$	$1.98 \pm 0.01$	Y
A2065	$0.91 \pm 0.02$	$3.18 \pm 0.16$	$2.29 \pm 0.12$	$5.24 \pm 0.01$	Y
A2199	$0.82 \pm 0.01$	$0.83 \pm 0.01$	$1.64 \pm 0.05$	$3.13 \pm 0.01$	Y
A0262	$0.59 \pm 0.02$	$0.49 \pm 0.01$	$0.58 \pm 0.07$	$0.80 \pm 0.01$	Y
A2626	$0.85 \pm 0.03$	$1.60 \pm 0.03$	$1.81 \pm 0.14$	$1.68 \pm 0.01$	Y
A2657	$0.78 \pm 0.05$	$3.68 \pm 0.95$	$1.40 \pm 0.29$	$1.59 \pm 0.01$	Y
A3112	$1.01 \pm 0.02$	$0.76 \pm 0.01$	$3.18 \pm 0.17$	$4.33 \pm 0.01$	Y
A3558	$0.83 \pm 0.05$	$2.93 \pm 0.14$	$1.70 \pm 0.31$	$4.97 \pm 0.01$	Y
A3581	$0.65 \pm 0.02$	$0.66 \pm 0.01$	$0.79 \pm 0.06$	$0.77 \pm 0.01$	Y
A4059	$0.82 \pm 0.01$	$1.32 \pm 0.05$	$1.64 \pm 0.14$	$3.32 \pm 0.01$	Y
A0478	$1.11 \pm 0.04$	$0.81 \pm 0.01$	$4.19 \pm 0.49$	$11.93 \pm 0.01$	Y
A0496	$0.90 \pm 0.01$	$0.84 \pm 0.01$	$2.11 \pm 0.19$	$5.11 \pm 0.03$	Y
S1101	$0.80 \pm 0.03$	$0.73 \pm 0.01$	$1.51 \pm 0.17$	$2.03 \pm 0.02$	Y
AWM 7	$0.77 \pm 0.03$	$0.81 \pm 0.04$	$1.31 \pm 0.15$	$1.35 \pm 0.01$	Y
EXO0422	$0.76 \pm 0.02$	$0.50 \pm 0.02$	$1.28 \pm 0.12$	$1.22 \pm 0.01$	Y
Hercules	$0.67 \pm 0.07$	$1.58 \pm 0.12$	$0.88 \pm 0.29$	$0.71 \pm 0.01$	Y
HydraA	$0.85 \pm 0.01$	$0.59 \pm 0.01$	$1.85 \pm 0.08$	$3.42 \pm 0.01$	Y
MKW3S	$0.85 \pm 0.06$	$1.41 \pm 0.04$	$1.80 \pm 0.35$	$2.22 \pm 0.01$	Y
MKW4	$0.60 \pm 0.04$	$0.57 \pm 0.01$	$0.62 \pm 0.13$	$0.47 \pm 0.01$	Y
MKW8	$0.61 \pm 0.02$	$1.22 \pm 0.05$	$0.68 \pm 0.08$	$0.59 \pm 0.01$	Y
A1060	$0.69 \pm 0.02$	$3.67 \pm 0.39$	$0.93 \pm 0.06$	$0.96 \pm 0.01$	N
A1651	$1.01 \pm 0.02$	$3.80 \pm 0.16$	$3.22 \pm 0.19$	$6.40 \pm 0.01$	N
A2063	$0.67 \pm 0.02$	$2.63 \pm 0.50$	$0.87 \pm 0.08$	$2.08 \pm 0.01$	N
A2589	$0.79 \pm 0.02$	$2.57 \pm 0.13$	$1.46 \pm 0.13$	$2.12 \pm 0.01$	N
A3158	$0.86 \pm 0.03$	$7.31 \pm 0.45$	$1.94 \pm 0.18$	$3.70 \pm 0.02$	N
A3391	$1.08 \pm 0.03$	$6.79 \pm 0.12$	$3.74 \pm 0.45$	$2.56 \pm 0.02$	N
A3571	$1.04 \pm 0.02$	$2.42 \pm 0.14$	$3.33 \pm 0.32$	$6.08 \pm 0.02$	N
A3827	$1.11 \pm 0.07$	$5.93 \pm 0.72$	$4.30 \pm 0.28$	$7.84 \pm 0.01$	N
A0399	$1.51 \pm 0.03$	$7.92 \pm 0.15$	$10.40 \pm 0.58$	$9.00 \pm 0.32$	N
A0400	$0.58 \pm 0.03$	$1.90 \pm 0.19$	$0.55 \pm 0.08$	$0.52 \pm 0.01$	N
A4010	$0.89 \pm 0.04$	$1.49 \pm 0.06$	$2.00 \pm 0.28$	$2.77 \pm 0.04$	N
AWM 4	$0.66 \pm 0.03$	$2.33 \pm 0.14$	$0.85 \pm 0.11$	$0.88 \pm 0.01$	N
Triangulum	$1.27 \pm 0.05$	$9.64 \pm 0.79$	$6.60 \pm 0.70$	$10.38 \pm 0.02$	N
IIIZw54	$0.72 \pm 0.03$	$5.11 \pm 0.62$	$1.08 \pm 0.14$	$1.15 \pm 0.01$	N

\* “cc” denotes cool core, “Y” denotes cool-core clusters, and “N” denote non-cool-core clusters.

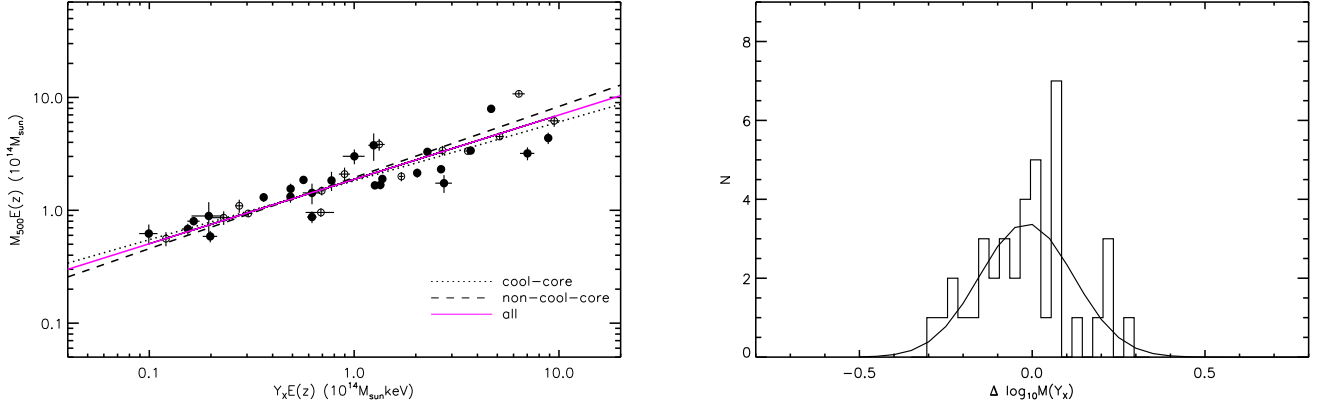


Fig. 7.— Left panel:  $Y_X$  is the product of the X-ray temperature  $T_{(0.2-0.5)r_{500}}$  and gas mass  $M_g$ . Right panel: Histogram of the residuals from the  $M_{500}$ - $Y_X$  relation in log space. This raw scatter is well described by a Gaussian fit of  $\sigma_{M(Y_X)} = 0.13$  dex.

Table 3: Comparisons of four different fit methods for the  $M_{500}$ - $T$  relation. The relations are given in the form:  $\log_{10}(Y) = A + B \cdot \log_{10}(X)$ . For each method, we list the normalization parameter  $A$ , and the slop  $B$ .

Method	$B$	$A$
BCES(Y X)	$2.22 \pm 0.42$	$13.85 \pm 0.13$
BCES(X Y)	$1.94 \pm 0.18$	$13.28 \pm 0.07$
BCES Bisector	$1.94 \pm 0.17$	$13.12 \pm 0.01$
BCES Orthogonal	$1.99 \pm 0.20$	$13.15 \pm 0.08$

Table 4: Summary of the fits to the mass scaling relations. The relations are given in the form:  $\log_{10}(Y) = A + B \cdot \log_{10}(X)$ . For each relation, we list the normalization parameter  $A$ , and the slope  $B$ . In addition to the results for all the sample, we also list the results both for the CCC sub-sample, and the NCCC sub-sample.

$Y$	$X$	Number of clusters	$B$	$A$	comments
$\frac{M_{500}}{M_{\odot}} E(z)$	$\frac{T}{\text{keV}}$	39	$1.94 \pm 0.17$	$13.12 \pm 0.10$	ALL
		25	$1.85 \pm 0.22$	$13.17 \pm 0.12$	CCCs
		14	$2.03 \pm 0.26$	$13.08 \pm 0.15$	NCCCs
$\frac{M_{500}}{M_{\odot}} E(z)$	$\frac{M_g}{M_{\odot}} E(z)$	39	$0.79 \pm 0.07$	$3.67 \pm 0.95$	ALL
		25	$0.72 \pm 0.09$	$4.66 \pm 1.17$	CCCs
		14	$0.89 \pm 0.11$	$2.36 \pm 1.41$	NCCCs
$\frac{L_{\text{bol}}}{\text{erg s}^{-1}} E(z)^{-1}$	$\frac{M_{500}}{M_{\odot}} E(z)$	39	$1.73 \pm 0.16$	$19.68 \pm 2.26$	ALL
		25	$2.03 \pm 0.22$	$15.35 \pm 3.19$	CCCs
		14	$1.38 \pm 0.17$	$24.58 \pm 2.33$	NCCCs
$\frac{M_{500}}{M_{\odot}} E(z)$	$\frac{Y_X}{M_{\odot} \text{ keV}} E(z)$	39	$0.57 \pm 0.04$	$6.29 \pm 0.58$	ALL
		25	$0.52 \pm 0.06$	$5.47 \pm 0.80$	CCCs
		14	$0.63 \pm 0.06$	$6.95 \pm 0.76$	NCCCs

Table 5: Comparison of the mass relations in our cluster sample. We list the results for the whole sample. The raw scatters are derived by a Gaussian fit to the residual histograms. The intrinsic scatters are obtained from Eq. (10).

	self-similarity	$B$	$A$	scatter (dex)	intrinsic scatter (dex)
$M_{500}E(z)-T$	1.5	$1.94 \pm 0.17$	$13.12 \pm 0.10$	0.18	0.14
$L_{\text{bol}}E(z)^{-1}-M_{500}E(z)$	1.33	$1.73 \pm 0.16$	$19.68 \pm 2.26$	0.27	0.15
$M_{500}E(z)-M_gE(z)$	1.0	$0.79 \pm 0.07$	$3.67 \pm 0.95$	0.14	0.14
$M_{500}E(z)-Y_XE(z)$	0.6	$0.57 \pm 0.04$	$6.29 \pm 0.58$	0.13	0.13

Table 6: Recent results on the slopes of the scaling relations.

relation	slope	comments	reference
$L_{bol} - M_{500}$	$1.63 \pm 0.08$	115 clusters, $z = 0.1 - 1.3$ , core excised $L_{bol}$ , $r < 0.15r_{500}$	Maughan07
$L_{0.1-2.4} - M_{500}$	$1.82 \pm 0.13$	106 clusters, <i>ROSAT/ASCA</i>	Chen07
$L_{bol} - M_{500}$	$1.71 \pm 0.46$	24 clusters, <i>Chandra</i> , core excised $L_{bol}$ , $r < 100\text{kpc}$	Morandi07
$L_{bol} - M_{500}$	$2.33 \pm 0.70$	37 clusters, <i>XMM</i> , core corrected $L_{bol}$ , $r < 0.2r_{500}$	Zhang08
$L_{0.1-2.4} - M_{500}$	$1.76 \pm 0.13$	31 clusters, <i>XMM</i>	Arnaud10
$L_{bol} - M_{500}$	$1.51 \pm 0.09$	14 literature samples	Reichert11
$M_{500} - T$	$1.54 \pm 0.06$	106 clusters, <i>ROSAT/ASCA</i>	Chen07
$M_{500} - T$	$1.71 \pm 0.09$	10 clusters, $T_{0.1-0.5r_{200}}$ , <i>XMM</i>	Arnaud07
$M_{500} - T$	$1.74 \pm 0.09$	70 clusters, $z = 0.18 - 1.24$	O’Hara07
$M_{500} - T$	$1.65 \pm 0.26$	$T_{0.2-0.5r_{500}}$	Zhang08
$M_{500} - T$	$1.53 \pm 0.08$	17 clusters, $T_{0.15-1r_{500}}$ , <i>Chandra</i>	Vikhlinin09
$M_{500} - T$	$2.04 \pm 0.04$	238 clusters, <i>Chandra/ROSAT</i>	Mantz10
$M_{500} - T$	$1.76 \pm 0.08$	14 literature samples	Reichert11
$M_{500} - M_g$	$0.80 \pm 0.04$	10 clusters, <i>XMM</i>	Arnaud07
$M_{500} - M_g$	$0.81 \pm 0.07$	simulation	Nagai07
$M_{500} - M_g$	$0.91 \pm 0.08$	37 clusters, <i>XMM</i>	Zhang08
$M_{500} - Y$	$0.57 \pm 0.01$	simulation	Nagai07
$M_{500} - Y$	$0.59 \pm 0.01$	simulation	Fabjan11
$M_{500} - Y$	$0.56 \pm 0.03$	10 clusters, <i>XMM</i>	Arnaud07
$M_{500} - Y$	$0.57 \pm 0.03$	17 clusters, <i>Chandra</i>	Vikhlinin09
$M_{500} - Y$	$0.62 \pm 0.06$	37 clusters, <i>XMM</i>	Zhang08

The references are from top to bottom: Maughan et al. (2007), Chen et al. (2007), Morandi et al. (2007), Zhang et al. (2008), Arnaud et al. (2010), Reichert et al. (2011), Arnaud et al. (2007), O’Hara et al. (2007), Vikhlinin et al. (2009), Mantz et al. (2010), Nagai et al. (2007), Fabjan et al. (2011).

- Eckert, D., et al., 2012, A&A, 541, A57
- Ettori, S., Tozzi, P., Borgani, S., et al. 2004, A&A, 417, 13
- Fabjan, D., Borgani, S., Rasia, E., et al. 2011, MNRAS, 416, 801
- Fabricant, D., Lecar, M., & Gorenstein, P. 1980, ApJ, 241, 552
- Finoguenov, A., Arnaud, M., David, L. p., 2001, ApJ, 555, 191
- Giodini, S., et al., 2009, ApJ, 703, 982
- Grandi, S. D., Böhringer, H., Guzzo, L., et al. 1999, 514, 148
- Hudson, D. S., Mittal, R., Reiprich, T. H., et al. 2010, A&A, 513, A37
- Jia, S. M., Chen, Y., Lu, F. J., et al. 2004, A&A, 423, 65
- Jia, S. M., Chen, Y. & Chen, L. 2006, ChJAA, Vol. 6, 181
- Kaastra, J. S., 1992, An X-ray Spectral Code for Optically Thin Plasma (Internal Sron-Leiden Report, update version 2.0)
- Kravtsov, A. V., Nagai, D., & Vikhlinin, A. A. 2005, ApJ, 625, 588
- Kravtsov, A. V., Vikhlinin, A. A., & Nagai, D. 2006, ApJ, 650, 128
- Li, C. K., Jia, S. M., Chen, Y., et al. 2013, in preparation
- Mantz, A., Allen, S. W., Ebeling, H., et al. 2010, MNRAS, 406, 1773
- Maughan, B. J. 2007, ApJ, 668, 772
- Mewe, R., Gronenschild, E. H. B. M., & Van den Oord, G. H. J. 1985, A&A, 62, 197
- Morrison, R., McCammon, D. 1983, ApJ, 270, 119
- Morandi, A., Ettori, S., & Moscardini, L. 2007, MNRAS, 379, 518
- Nagai, D., Kravtsov, A. V., & Vikhlinin, A. 2007, ApJ, 668, 1
- O'Hara, T.B., Mohr, J.J., Bialek, J.J., Evrard, A.E., 2006, ApJ, 639, 640
- Okabe, N., Zhang, Y., Finoguenov, A., et al. 2010, ApJ, 721, 875
- Poole, G. B., Babul, A., McCarthy, I. G., et al. 2007, MNRAS, 380, 437



- Pratt, G. W., Croston, J. H., Arnaud, M., et al. 2009, A&A, 498, 361
- Rafferty, D.A., McNamara, B. R., Nulsen, P. E. J., et al. 2006, ApJ, 652, 216
- Rasia, E., Mazzotta, P., Evrard, A., et al. 2011, ApJ, 729, 45
- Reiprich, T. H., & Böhringer, H. 2002, ApJ, 567, 716
- Reichert, A., Böhringer, H., Fassbender, R., & Mülleger, M. 2011, A&A, 535, A4
- Sanderson, A. J. R., Ponman, T. J., Finoguenov, A. et al. 2003, MNRAS, 340, 989
- Sanderson, A. J. R., Ponman, T. J., & O’Sullivan, E. 2006, MNRAS, 372, 1496
- Sarazin, C. L., 1988, X-ray Emission From Clusters of Galaxies. Cambridge University Press
- Smith, G. P., Kneib, J. P., Smail, I., et al. 2005, MNRAS, 359, 417
- Snowden, S. L. et al., 1997, ApJ, 485, 125
- Stanek, R., Evrard, A. E., Böhringer, H., et al. 2006, ApJ, 648, 956
- Stanek, R., Rasia, E., Evrard, A. E., et al. 2010, ApJ, 715, 1508
- Thomas, H. R., Böhringer, H., 2002, 567, 716
- Vikhlinin, A., Kravtsov, A., Forman, W., et al. 2006, ApJ, 640, 691
- Vikhlinin, A., Burenin, R., Forman, W. R., et al. 2007, in Heating vs. Cooling in Galaxies and Clusters of Galaxies, ed. H. Böhringer, G. W. Pratt, & P. Schuecker, 48
- Vikhlinin, A., et al. 2009, ApJ, 692, 1060
- Voit, G. M., & Donahue, M. 2005, ApJ, 634, 955
- Xue, Y. J., Böhringer, H., & Matsushita, K., 2004, A&A, 542, 578
- Zhang, Y. Y., Böhringer, H., Finoguenov, A., et al. 2006, A&A, 456, 55
- Zhang, Y. Y., Finoguenov, A., Böhringer, H., et al. 2007, A&A, 467, 437
- Zhang, Y. Y., Finoguenov, A., Böhringer, H., et al. 2008, A&A, 482, 451